Supplementary Information

Modelling Charge Transport and Electro-Optical Characteristics of Quantum Dot Light-Emitting Diodes

Sung-Min Jung[1*], Tae Hoon Lee[1], Sang Yun Bang[1], Soo Deok Han[1], Dong-Wook Shin[1], Sanghyo Lee[1], Hyung Woo Choi[1], Yo-Han Suh[1], Xiang-Bing Fan[1], Jeong-Wan Jo[1], Shijie Zhan[1], Jiajie Yang[1], Chatura Samarakoon[1], Yoonwoo Kim[1], Luigi G. Occhipinti[1], Gehan Amaratunga[1], and Jong Min Kim[1*]

[1]*Electrical Engineering Division, Department of Engineering, University of Cambridge, 9 JJ Thomson Ave, Cambridge, CB3 0FA, United Kingdom*

* Corresponding authors: Sung-Min Jung and Jong Min Kim

E-mail addresses: sj569@cam.ac.uk, jmk71@cam.ac.uk

I. Supplementary Methods

Tunnelling probability. When a carrier crosses a tunnelling barrier formed by a QD shell of thickness t_s, the tunnelling probability is described as Supplementary Eq. (1).[1, 2]

$$T_{\mathrm{bs}} = \begin{cases} 1 , & \Delta E^{\mathrm{S}} < 0 \\ \exp\left(-\frac{2\pi}{h} t_{\mathrm{s}} \sqrt{8 m_{\mathrm{s}}^{*} \Delta E^{\mathrm{S}}}\right), & \Delta E^{\mathrm{S}} \geq 0 \end{cases} \tag{1}$$

Here, ΔE^{S} is the energy barrier height defined by $\Delta E^{\mathrm{S}} = E^{\mathrm{S}} - E$, where E^S and E are the energy-levels of the shell and the carrier, respectively. h is the Planck's constant and m_s^* is the effective mass of the carrier in the QD shell. The tunnelling probability can be used for the calculation of the tunnelling barriers of QD shells at the interfaces between charge transport layers and QD layer, and the calculation of tunnelling barrier of QD shells between two neighbouring QDs for obtaining the tunnelling frequencies.

Tunnelling frequency. The tunnelling frequency for a given carrier which oscillates between two neighbouring QDs is described by the following equation.[3]

$$\nu = \frac{v_{\mathrm{th}}}{2 d_{\mathrm{QD}}} T_{\mathrm{bs}} \tag{2}$$

Here, v_{th} is a thermal velocity of a given carrier in QD core and d_{QD} is the diameter of QD. The thermal velocity of the carrier is expressed as $v_{\mathrm{th}} = (2k_{\mathrm{B}}T/m_{\mathrm{c}}^*)^{1/2}$ for the Boltzmann constant k_B, the absolute temperature T, and the effective mass m_c^* of the given charge carrier in QD core. T_{bs} is the tunnelling probability of the QD shells between two neighbouring QDs, which is calculated by Supplementary Eq. (1).

II. Supplementary Figures

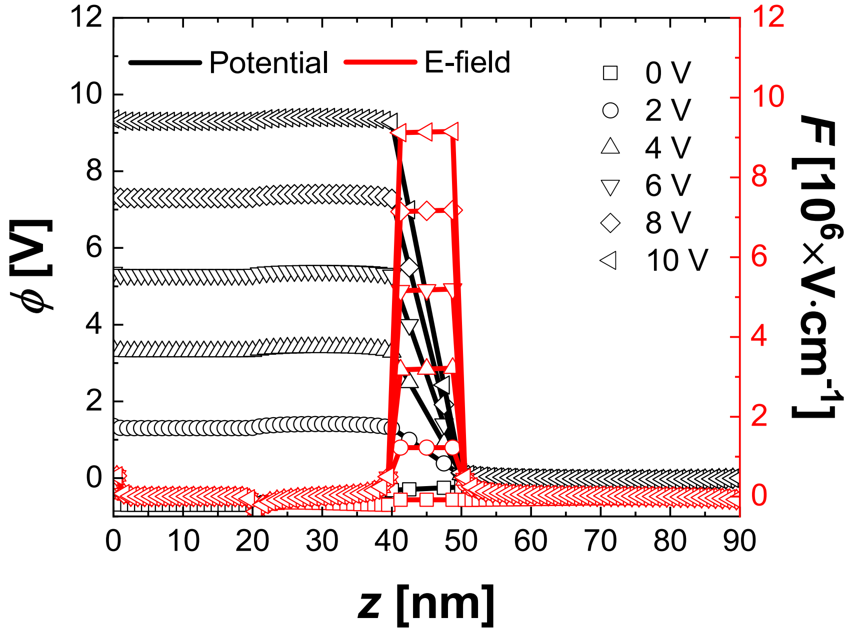

Supplementary Figure 1. Potential and electric field distributions across the entire QD-LED device under different applied voltages.

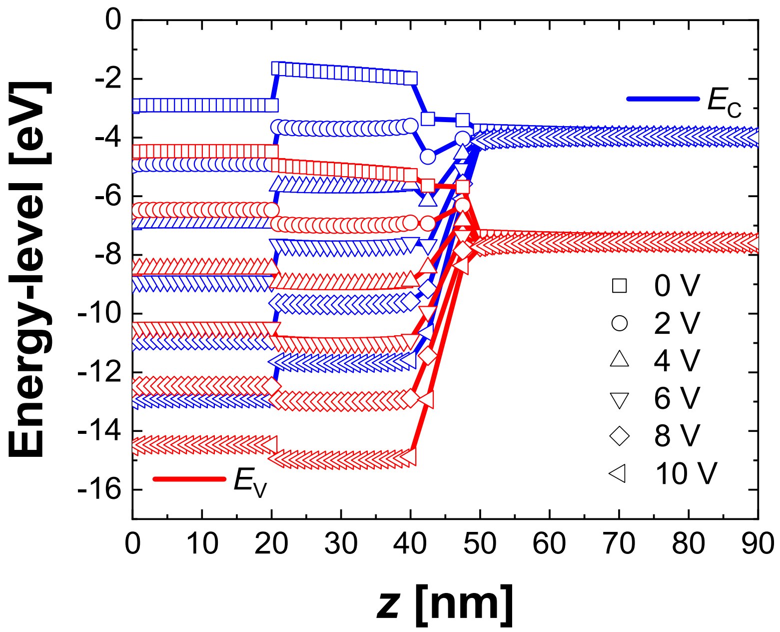

Supplementary Figure 2. Energy-level distributions across the entire QD-LED device under different applied voltages.

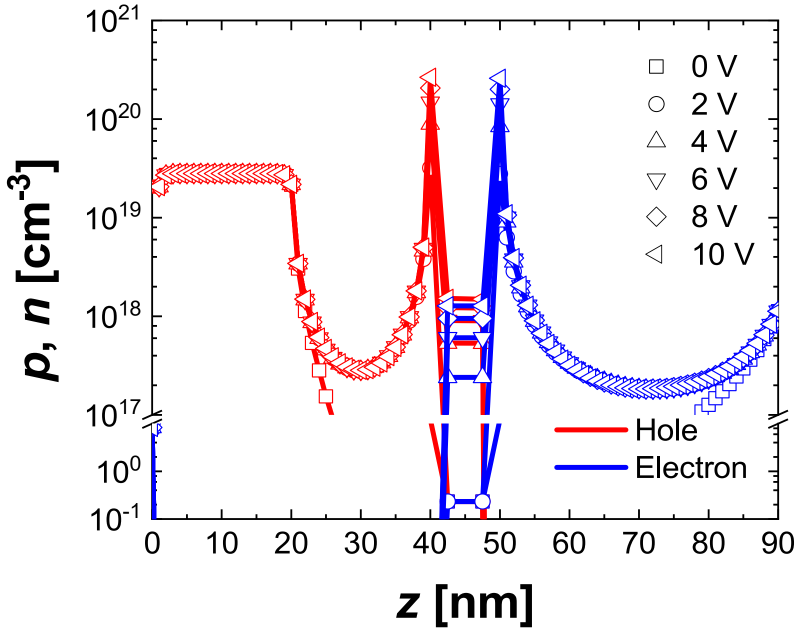

Supplementary Figure 3. Hole and electron densities across the entire QD-LED device under different applied voltages.

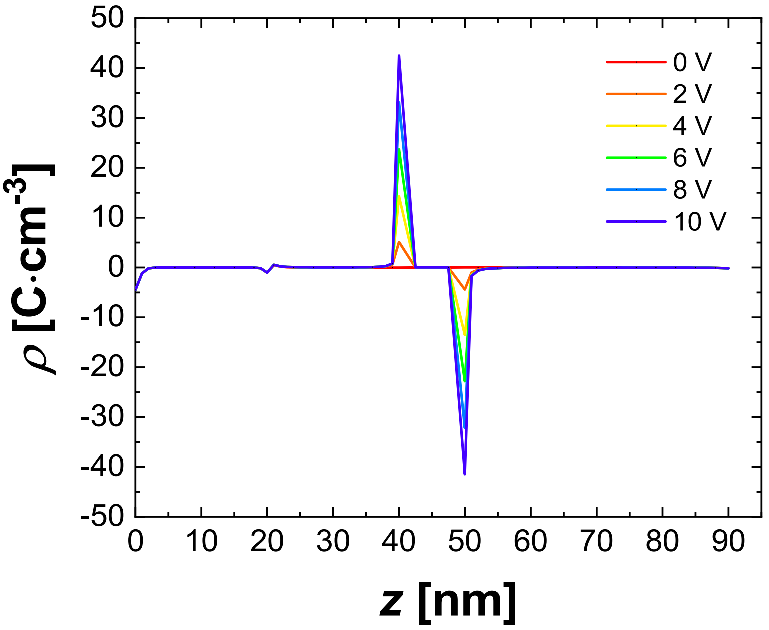

Supplementary Figure 4. Charge density distributions across the entire QD-LED device under different applied voltages. The positive charges and the negative charges are gathered on the surfaces of HTL and ETL facing QD layer so that the electric fields are formed within the QD layer.

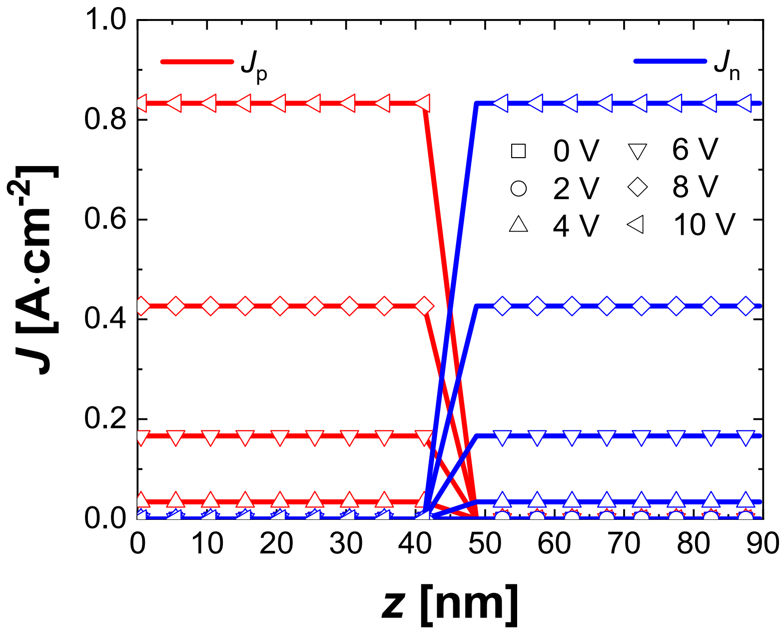

Supplementary Figure 5. Hole and electron current density distributions across the entire QD-LED device. Hole current density is dominant in the HIL/HTL region, while electron current density is dominant in the ETL region. Hole and electron current densities are diminished by the recombination process in the QD region. Total current density, which is the sum of hole and electron current densities, is constant over the entire device.

III. Supplementary Tables

Supplementary Table 1. Material parameters of QDs used for the simulation.

QD Parameters	**Core**	**Shell**
Materials	CdSe	ZnS
Diameter/Thickness [nm]	4.0	0.5
Dielectric constant, ε_r	9.4[4]	
Hole mobility, μ_{p0}^{QD} [cm^2 V^{-1} s^{-1}] @ F_0=5.0 [MV cm^{-1}]	1.0×10^{-6}[5]	
Electron mobility, μ_{n0}^{QD} [cm^2 V^{-1} s^{-1}] @ F_0=5.0 [MV cm^{-1}]	2.0×10^{-6}[5]	
Centre wavelength, λ_0 [nm]	545	
Hole effective mass, m_p^*/m_0[a]	0.45[6]	0.60[7]
Electron effective mass, m_n^*/m_0	0.13[6]	0.19[7]
LUMO [eV]	-3.66[b]	-3.28[8]
HOMO [eV]	-5.94[b]	-6.82[8]
Langevin radiative recombination strength, γ [cm^3 s^{-1}]	0.58×10^{-12}[9]	
Charge injection mobility, $\alpha_p = \alpha_n$ [cm^2 V^{-1} s^{-1}]	3.0×10^{-9}	

[a]m_0 is an electron mass in free space.
[b]The LUMO level of QD is obtained from the charge balance condition in energy-level, and the HOMO level is obtained by LUMO - E_G^{QD} where $E_G^{QD} = hc/\lambda_0$ for the Planck constant h, the speed of light c and peak wavelength λ_0 of light emitted from QD.

Supplementary Table 2. Materials and device parameters of transport layers and electrodes of QD-LEDs used in the simulation.

Parameters	Anode	HIL	HTL	ETL	Cathode
Materials	ITO	PEDOT:PSS	TFB	ZnO	Al
Thickness [nm]		20	20	40	
Dielectric constant, ε_r		3.0[10]	3.5[11]	8.5[12]	
Hole mobility, μ_p [$cm^2\ V^{-1}\ s^{-1}$]		0.322×10^{-3}[10]	2.0×10^{-3}[13]		
Electron mobility, μ_n [$cm^2\ V^{-1}\ s^{-1}$]				2.0×10^{-3}[14]	
Hole effective mass, m_p^*/m_0		1.0	1.0	0.59[15]	
Electron effective mass, m_n^*/m_0		1.0	1.0	0.24[15]	
Doping type		p-type	p-type	n-type	
Doping concentrations, N_a, N_d [cm^{-3}]		2.81×10^{19}[16]	1.00×10^{17}[3]	1.00×10^{17}[3]	
Work-functions, ϕ [eV]	4.70[17]				4.06[18]
Conduction band edge, E_{C0} [eV]		-3.6[19]	-2.60	-4.00[12,18]	
Valance band edge, E_{V0} [eV]		-5.17[19]	-5.60[20]	-7.40[12,18]	
SRH recombination lifetime, $\tau_p = \tau_n$ [μs]		1.2[3,19]	1.2[3,19]	1.2[3,19]	

Supplementary References

[1] Yang, K., East, J. R. & Haddad, G. I. Numerical modeling of abrupt heterojunctions using a thermionic-field emission boundary condition. *Solid State Electron.* **36**, 321-330 (1993).

[2] Jung, S. *et al.* Modeling electrical percolation to optimize the electromechanical properties of CNT/polymer composites in highly stretchable fiber strain sensors. *Sci. Rep.* **9**, 20376 (2019).

[3] Kumar, B., Campbell, S. A. & Ruden, P. P. Modeling charge transport in quantum dot light emitting devices with NiO and ZnO transport layers and Si quantum dots. *J. Appl. Phys.* **114**, 1-6 (2013).

[4] Canali, C., Nava, F. & Ottaviani, G. Hole and electron drift velocity in CdSe at room temperature. *Solid State Commun.* **11**, 105-107 (1972).

[5] Kathirgamanathan, P., Kumaraverl, M., Bramananthan, N. & Ravichandran, S. High efficiency and highly saturated red emitting inverted quantum dot devices (QLEDs): optimisation of their efficiencies with low temperature annealed sol–gel derived ZnO as the electron transporter and a novel high mobility hole transporter and thermal annealing of the devices. *J. Mater. Chem. C* **6**, 11622-11644 (2018).

[6] Kippeny, T., Swafford, L. A. & Rosenthal, S. J. Semiconductor nanocrystals: a powerful visual aid for introducing the particle in a box. *J. Chem. Educ.* **79**, 1094-1100 (2002).

[7] Karazhanov, S. Z. & Voon, L. C. L. Y. Ab initio studies of the band parameters of III–V and II–VI zinc-blende semiconductors. *Semiconductors* **39**, 161-173 (2004).

[8] Cerdan-Pasaran, A. *et al.* Photovoltaic properties of multilayered quantum dot/quantum rod-sensitized TiO2 solar cells fabricated by SILAR and electrophoresis. *Phys. Chem. Chem. Phys.* **17**, 18590-18599 (2015).

[9] Liang, C. *et al.* Modeling and simulation of bulk heterojunction polymer solar cells. *Sol. Energy Mater. Sol. Cells* **127**, 67-86 (2014).

[10] Xu, B. *et al.* Functional solid additive modified PEDOT:PSS as an anode buffer layer for enhanced photovoltaic performance and stability in polymer solar cells. *Sci. Rep.* **7**, 1-12 (2017).

[11] Han, Y. J., An, K., Kang, K. T., Ju, B.-K. & Cho, K. H. Optical and electrical analysis of annealing temperature of high molecular weight hole transport layer for quantum-dot light-emitting diodes. *Sci. Rep.* **9**, 1-9 (2019).

[12] Vallisree, S., Thangavel, R. & Lenka, T. R. Modelling, simulation, optimization of

Si/ZnO and Si/ZnMgO heterojunction solar cells. *Mater. Res. Express* **6**, 025910 (2018).

[13] Zhao, Y. *et al.* Composite hole transport layer consisting of high-mobility polymer and small molecule with deep-lying HOMO level for efficient quantum dot light-emitting diodes. *IEEE Electr. Device L.* **41** (2020).

[14] Wang, F. *et al.* Achieving balanced charge injection of blue quantum dot light-emitting diodes through transport layer doping strategies. *J. Phys. Chem. Lett.* **10**, 960-965 (2019).

[15] Norton, D. P. *et al.* ZnO: growth, doping & processing. *Mater. Today* **7**, 34-40 (2004).

[16] Yan, F., Parrott, E. P. J., Ung, B. S.-Y. & Pickwell-MacPherson, E. Solvent doping of PEDOT/PSS: Effect on terahertz optoelectronic properties and utilization in terahertz devices. *J. Phys. Chem. C* **119**, 6813-6818 (2015).

[17] Park, Y., Choong, V., Gao, Y., Hsieh, B. R. & Tang, C. W. Work function of indium tin oxide transparent conductor measured by photoelectron spectroscopy. *Appl. Phys. Lett.* **68**, 2699-2701 (1996).

[18] Kim, J. *et al.* ZnO nanowire-embedded Schottky diode for effective UV detection by the barrier reduction effect. *Nanotechnology* **21**, 115205 (2010).

[19] Vahabzad, F., Rostami, A., Dolatyari, M., Rostami, G. & Amiri, I. S. Solution-processed QD-LEDs in visible range: Modulation bandwidth enhancement. *Physica B: Condensed Matter* **574**, 411667 (2019).

[20] Kim, T. *et al.* Efficient and stable blue quantum dot light-emitting diode. *Nature* **586**, 385-389 (2020).